Cite as: A. Chandrashekar *et al.*, *Science* 10.1126/science.abc4776 (2020).

SARS-CoV-2 infection protects against rechallenge in rhesus macaques

Abishek Chandrashekar[1]*, Jinyan Liu[1]*, Amanda J. Martinot[1,2]*, Katherine McMahan[1]*, Noe B. Mercado[1]*, Lauren Peter[1]*, Lisa H. Tostanoski[1]*, Jingyou Yu[1]*, Zoltan Maliga[3], Michael Nekorchuk[4], Kathleen Busman-Sahay[4], Margaret Terry[4], Linda M. Wrijil[2], Sarah Ducat[2], David R. Martinez[5], Caroline Atyeo[3,6], Stephanie Fischinger[6], John S. Burke[6], Matthew D. Slein[6], Laurent Pessaint[7], Alex Van Ry[7], Jack Greenhouse[7], Tammy Taylor[7], Kelvin Blade[7], Anthony Cook[7], Brad Finneyfrock[7], Renita Brown[7], Elyse Teow[7], Jason Velasco[7], Roland Zahn[8], Frank Wegmann[8], Peter Abbink[1], Esther A. Bondzie[1], Gabriel Dagotto[1,3], Makda S. Gebre[1,3], Xuan He[1], Catherine Jacob-Dolan[1,3], Nicole Kordana[1], Zhenfeng Li[1], Michelle A. Lifton[1], Shant H. Mahrokhian[1], Lori F. Maxfield[1], Ramya Nityanandam[1], Joseph P. Nkolola[1], Aaron G. Schmidt[6,9], Andrew D. Miller[10], Ralph S. Baric[5], Galit Alter[6,9], Peter K. Sorger[3], Jacob D. Estes[4], Hanne Andersen[7], Mark G. Lewis[7], Dan H. Barouch[1,6,9]†

[1]Center for Virology and Vaccine Research, Beth Israel Deaconess Medical Center, Harvard Medical School, Boston, MA 02215, USA. [2]Tufts University Cummings School of Veterinary Medicine, North Grafton, MA 01536, USA. [3]Harvard Medical School, Boston, MA 02115, USA. [4]Oregon Health & Sciences University, Beaverton, OR 97006, USA. [5]University of North Carolina, Chapel Hill, NC 27599, USA. [6]Ragon Institute of MGH, MIT, and Harvard, Cambridge, MA 02139, USA. [7]Bioqual, Rockville, MD 20852, USA. [8]Janssen Vaccines & Prevention BV, Leiden, Netherlands. [9]Massachusetts Consortium on Pathogen Readiness, Boston, MA 02215, USA. [10]Cornell University College of Veterinary Medicine, Ithaca, NY 14853, USA.

*These authors contributed equally to this work.

†Corresponding author. Email: dbarouch@bidmc.harvard.edu

An understanding of protective immunity to SARS-CoV-2 is critical for vaccine and public health strategies aimed at ending the global COVID-19 pandemic. A key unanswered question is whether infection with SARS-CoV-2 results in protective immunity against re-exposure. We developed a rhesus macaque model of SARS-CoV-2 infection and observed that macaques had high viral loads in the upper and lower respiratory tract, humoral and cellular immune responses, and pathologic evidence of viral pneumonia. Following initial viral clearance, animals were rechallenged with SARS-CoV-2 and showed 5 $\log_{10}$ reductions in median viral loads in bronchoalveolar lavage and nasal mucosa compared with primary infection. Anamnestic immune responses following rechallenge suggested that protection was mediated by immunologic control. These data show that SARS-CoV-2 infection induced protective immunity against re-exposure in nonhuman primates.

The explosive spread of the COVID-19 pandemic has made the development of countermeasures an urgent global priority (*1*–*8*). However, our understanding of the immunopathogenesis of SARS-CoV-2 is currently very limited. In particular, it is currently not known whether SARS-CoV-2 infection induces natural immunity that protects against re-exposure in humans. Such information is critical for vaccine strategies, epidemiologic modeling, and public health approaches. To explore this question, we developed a rhesus macaque model of SARS-CoV-2 infection, and we assessed virologic, immunologic, and pathologic features of infection as well as protective immunity against rechallenge.

Virology and immunology of SARS-CoV-2 infection in rhesus macaques

We inoculated 9 adult rhesus macaques (6-12 years old) with a total of 1.1×10^6 PFU (Group 1; N = 3), 1.1×10^5 PFU (Group 2; N = 3), or 1.1×10^4 PFU (Group 3; N = 3) SARS-CoV-2, administered as 1 ml by the intranasal (IN) route and 1 ml by the intratracheal (IT) route. Following viral challenge, we assessed viral RNA levels by RT-PCR in multiple anatomic compartments. We observed high levels of viral RNA in bronchoalveolar lavage (BAL) (Fig. 1A) and nasal swabs (NS) (Fig. 1B), with a median peak of 6.56 (range 5.32-8.97) $\log_{10}$ RNA copies/ml in BAL and a median peak of 7.00

(range 5.06-8.55) $\log_{10}$ RNA copies/swab in NS. Viral RNA in NS increased in all animals from day 1 to day 2, suggesting viral replication. Viral RNA peaked on day 2 and typically resolved by day 10-14 in BAL and by day 21-28 in NS. Following day 2, viral loads in BAL and NS appeared comparable in all groups regardless of dose. Viral RNA was undetectable in plasma (fig. S1). Animals exhibited modestly decreased appetite and responsiveness suggestive of mild clinical disease (fig. S2) as well as mild transient neutropenia and lymphopenia in the high dose group (fig. S3), but fever, weight loss, respiratory distress, and mortality were not observed.

To help differentiate input challenge virus from newly replicating virus, we developed an RT-PCR assay to assess E gene subgenomic mRNA (sgmRNA). E gene sgmRNA reflects viral replication cellular intermediates that are not packaged into virions and thus represent putative replicating virus in cells (*9*). Compared with total viral RNA (Fig. 1B), sgmRNA levels were lower in NS on day 1 with a median of 5.11 (range <1.70-5.94) $\log_{10}$ sgmRNA copies/swab, but then increased by day 2 to a median of 6.50 (range 4.16-7.81) $\log_{10}$ sgmRNA copies/swab (Fig. 1C).

We next evaluated SARS-CoV-2-specific humoral and cellular immune responses in these animals. All 9 macaques developed binding antibody responses to the SARS-CoV-2 Spike (S) protein by ELISA (Fig. 2A) and neutralizing antibody (NAb) responses using both a pseudovirus neutralization assay (*10*) (Fig. 2B) and a live virus neutralization assay (*11*, *12*) (Fig. 2C). NAb titers of approximately 100 were observed in all animals on day 35 regardless of dose group (range 83-197 by the pseudovirus neutralization assay and 35-326 by the live virus neutralization assay). Antibody responses of multiple subclasses were observed against the receptor binding domain (RBD), the prefusion S ectodomain (S), and the nucleocapsid (N), and antibodies exhibited diverse effector functions, including antibody-dependent complement deposition (ADCD), antibody-dependent cellular phagocytosis (ADCP), antibody-dependent neutrophil phagocytosis (ADNP), and antibody-dependent NK cell degranulation (NK CD107a) and cytokine secretion (NK MIP1β, NK IFNγ) (*13*) (Fig. 2D). Cellular immune responses to pooled S peptides were observed in the majority of animals by IFN-γ ELISPOT assays on day 35, with a trend toward lower responses in the lower dose groups (Fig. 2E). Intracellular cytokine staining assays demonstrated induction of both S-specific CD8+ and CD4+ T cell responses (Fig. 2F).

SARS CoV-2 infection induces acute viral interstitial pneumonia in rhesus macaques

Only limited pathology data from SARS-CoV-2 infected humans are currently available. To assess the pathologic characteristics of SARS-CoV-2 infection in rhesus macaques, we inoculated 4 animals with 1.1×10^5 PFU virus by the IN and IT routes as above and necropsied them on day 2 (N = 2) and day 4 (N = 2) following challenge. Multiple regions of the upper respiratory tract, lower respiratory tract, gastrointestinal tract, lymph nodes, and other organs were harvested for virologic and pathologic analyses. High levels of viral RNA were observed in all nasal mucosa, pharynx, trachea, and lung tissues, and lower levels of virus were found in the gastrointestinal tract, liver, and kidney (fig. S4). Viral RNA was readily detected in paratracheal lymph nodes but was only sporadically found in distal lymph nodes and spleen (fig. S4).

Upper airway mucosae, trachea, and lungs were paraformaldehyde fixed, paraffin embeded, and evaluated by histopathology. On day 2 following challenge, both necropsied animals demonstrated multifocal regions of inflammation and evidence of viral pneumonia, including expansion of alveolar septae with mononuclear cell infiltrates, consolidation, and edema (Fig. 3, A and B). Regions with edema also contained numerous polymorphonuclear cells, predominantly neutrophils. Terminal bronchiolar epithelium was necrotic and sloughed with clumps of epithelial cells detected within airways and distally within alveolar spaces (Fig. 3, C and D) with formation of occasional bronchiolar epithelial syncytial cells (Fig. 3E). Hyaline membranes were occasionally observed within alveolar septa, consistent with damage to type I and type II pneumocytes (Fig. 3F). Diffusely reactive alveolar macrophages filled alveoli, and some were multinucleated and labeled positive for nucleocapsid by immunohistochemistry (Fig. 3G). Alveolar lining cells (pneumocytes) also prominently labeled positive for nucleocapsid (Fig. 3H).

Multifocal clusters of virus infected cells were present throughout the lung parenchyma, as detected by immunohistochemistry and in situ RNA hybridization (RNAscope) (*14*, *15*) (Fig. 3I). Both positive-sense and negative-sense viral RNA was observed by RNAscope (fig. S5), suggesting viral replication in lung tissue. The dense inflammatory infiltrates included polymorphonuclear cells detected by endogenous myeloperoxidase staining (MPO), CD68 and CD163 positive macrophages, CD4+ and CD8+ T lymphocytes, and diffuse up-regulation of the type 1 interferon gene MX1 (fig. S6). SARS-CoV-2 infection led to a significant increase in polymorphonuclear cell infiltration of lung alveoli compared with uninfected animals (P = 0.0286) as well as extensive MX1 staining in approximately 30% of total lung tissue (P = 0.0286) (fig. S7). Inflammatory infiltrates were also detected in the respiratory epithelial submucosa of larger airways with transmigration of inflammatory cells into bronchiole lumen (Fig. 3J). Ciliated epithelial cells also stained positive for both SARS CoV-2 RNA (Fig. 3K) and SARS nucleocapsid

(Fig. 3L). By day 4 following infection, the extent of inflammation and viral pneumonia had diminished, but virus was still detected in lung parenchyma and neutrophil infiltration and type 1 interferon responses persisted (fig. S7).

To further characterize infected tissues, we performed cyclic immunofluorescence (CyCIF) imaging, a method for multiplex immunophenotyping of paraformaldehyde fixed tissue specimens (*16*). Tissues were stained for nucleocapsid (SARS-N), pan-cytokeratin (to identify epithelial cells), Iba-1 (ionized calcium binding adaptor as a pan-macrophage marker), CD68 (monocyte/macrophage marker), and CD206 (macrophage marker), in addition to a panel of markers to identify other immune cells and anatomical structures (table S1), and counterstaining for DNA to label all nuclei. Foci of virus infected cells were randomly dispersed throughout the lung and were variably associated with inflammatory infiltrates (Fig. 4, A to D). Some areas of parenchymal consolidation and inflammation contained little to no virus (Fig. 4A, arrows, and fig. S8). Virus infected cells frequently co-stained with pan-cytokeratin (Fig. 4, E to H), suggesting that they were alveolar epithelial cells (pneumocytes). Uninfected Iba-1+ CD68+ CD206+ activated macrophages were also frequently detected adjacent to virally infected epithelial cells (Fig. 4, E and I to K). These data demonstrate that SARS-CoV-2 induced multifocal areas of acute inflammation and viral pneumonia involving infected pneumocytes, ciliated bronchial epithelial cells, and likely other cell types.

Protective efficacy against rechallenge with SARS-CoV-2 in rhesus macaques

On day 35 following initial viral infection (Figs. 1 and 2), we rechallenged all 9 rhesus macaques with the same doses of SARS-CoV-2 that were utilized for the primary infection, namely 1.1×10^6 PFU (Group 1; N = 3), 1.1×10^5 PFU (Group 2; N = 3), or 1.1×10^4 PFU (Group 3; N = 3). We included 3 naïve animals as positive controls in the rechallenge experiment. Very limited viral RNA was observed in BAL on day 1 following rechallenge in two Group 1 animals and in one Group 2 animal, with no viral RNA detected at subsequent timepoints (Fig. 5A). In contrast, high levels of viral RNA were observed in the concurrently challenged naïve animals (Fig. 5A), as expected. Median peak viral loads in BAL were >5.1 $\log_{10}$ lower following rechallenge as compared with the primary challenge (P < 0.0001, two-sided Mann-Whitney test; Fig. 5B). Viral RNA following rechallenge was higher in NS compared with BAL, but exhibited dose dependence and rapid decline (Fig. 5C), and median peak viral loads in NS were still >1.7 $\log_{10}$ lower following rechallenge as compared with the primary challenge (P = 0.0011, two-sided Mann-Whitney test; Fig. 5D).

We speculated that the majority of virus detected in NS following rechallenge was input challenge virus, and we therefore assessed sgmRNA levels in NS following rechallenge. Low but detectable levels of sgmRNA were still observed in 4 of 9 animals in NS on day 1 following rechallenge, but sgmRNA levels declined quickly (Fig. 5E), and median peak sgmRNA levels in NS were >4.8 $\log_{10}$ lower following rechallenge as compared with the primary challenge (P = 0.0003, two-sided Mann-Whitney test; Fig. 5F). Consistent with these data, plaque assays in BAL and NS samples following rechallenge showed no recoverable virus and were lower than following primary infection (P = 0.009 and 0.002, respectively, two-sided Mann-Whitney tests; fig. S9). Moreover, little or no clinical disease was observed in the animals following rechallenge (fig. S10).

Following SARS-CoV-2 rechallenge, animals exhibited rapid anamnestic immune responses, including increased virus-specific ELISA titers (P = 0.0034, two-sided Mann-Whitney test), pseudovirus NAb titers (P = 0.0003), and live virus NAb titers (P = 0.0003) as well as a trend toward increased IFN-γ ELISPOT responses (P = 0.1837) by day 7 after rechallenge (Fig. 6). In particular, NAb titers were markedly higher on day 14 following rechallenge compared with day 14 following primary challenge (P < 0.0001, two-sided Mann-Whitney test) (fig. S11). All animals developed anamnestic antibody responses following rechallenge, regardless of the presence or absence of residual viral RNA or sgmRNA in BAL or NS, and thus we speculate that the protective efficacy against rechallenge was mediated by rapid immunologic control.

Discussion

Individuals who recover from certain viral infections typically develop virus-specific antibody responses that provide robust protective immunity against re-exposure, but some viruses do not generate protective natural immunity, such as HIV-1 (*17*). Human challenge studies for the common cold coronavirus 229E have suggested that there may be partial natural immunity (*18*). However, there is currently no data whether humans who have recovered from SARS-CoV-2 infection are protected from re-exposure (World Health Organization, Scientific Brief, April 24, 2020; https://www.who.int/news-room/commentaries/detail/immunity-passports-in-the-context-of-covid-19). This is a critical issue with profound implications for vaccine development, public health strategies, antibody-based therapeutics, and epidemiologic modeling of herd immunity. In this study, we demonstrate that SARS-CoV-2 infection in rhesus macaques provided protective efficacy against SARS-CoV-2 rechallenge.

We developed a rhesus macaque model of SARS-CoV-2 infection that recapitulates many aspects of human SARS-CoV-2 infection, including high levels of viral replication in the upper and lower respiratory tract (Fig. 1) and clear

pathologic evidence of viral pneumonia (Figs. 3 and 4). Histopathology, immunohistochemistry, RNAscope, and CyCIF imaging demonstrated multifocal clusters of virus infected cells in areas of acute inflammation, with evidence for virus infection of alveolar pneumocytes and ciliated bronchial epithelial cells. These data suggest the utility of rhesus macaques as a model for SARS-CoV-2 infection for testing vaccines and therapeutics and for studying immunopathogenesis, and our findings complement and extend recently published data in cynomolgus macaques (*19*). However, neither nonhuman primate model led to respiratory failure or mortality, and thus further research will be required to develop a nonhuman primate model of severe COVID-19 disease.

SARS-CoV-2 infection in rhesus macaques led to humoral and cellular immune responses (Fig. 2) and provided protection against rechallenge (Fig. 5). Residual low levels of subgenomic mRNA in nasal swabs in a subset of animals (Fig. 5) and anamnestic immune responses in all animals (Fig. 6) following SARS-CoV-2 rechallenge suggest that protection was mediated by immunologic control and likely was not sterilizing.

Given the near-complete protection in all animals following SARS-CoV-2 rechallenge, we were unable to determine immune correlates of protection in this study. SARS-CoV-2 infection in rhesus monkeys resulted in the induction of neutralizing antibody titers of approximately 100 by both a pseudovirus neutralization assay and a live virus neutralization assay, but the relative importance of neutralizing antibodies, other functional antibodies, cellular immunity, and innate immunity to protective efficacy against SARS-CoV-2 remains to be determined. Moreover, additional research will be required to define the durability of natural immunity.

In summary, SARS-CoV-2 infection in rhesus macaques induced humoral and cellular immune responses and provided protective efficacy against SARS-CoV-2 rechallenge. These data raise the possibility that immunologic approaches to the prevention and treatment of SARS-CoV-2 infection may in fact be possible. However, it is critical to emphasize that there are important differences between SARS-CoV-2 infection in macaques and humans, with many parameters still yet to be defined in both species, and thus our data should be interpreted cautiously. Rigorous clinical studies will be required to determine whether SARS-CoV-2 infection effectively protects against SARS-CoV-2 re-exposure in humans.

REFERENCES AND NOTES

1. F. Wu, S. Zhao, B. Yu, Y.-M. Chen, W. Wang, Z.-G. Song, Y. Hu, Z.-W. Tao, J.-H. Tian, Y.-Y. Pei, M.-L. Yuan, Y.-L. Zhang, F.-H. Dai, Y. Liu, Q.-M. Wang, J.-J. Zheng, L. Xu, E. C. Holmes, Y.-Z. Zhang, A new coronavirus associated with human respiratory disease in China. *Nature* **579**, 265–269 (2020). doi:10.1038/s41586-020-2008-3 Medline
2. P. Zhou, X.-L. Yang, X.-G. Wang, B. Hu, L. Zhang, W. Zhang, H.-R. Si, Y. Zhu, B. Li, C.-L. Huang, H.-D. Chen, J. Chen, Y. Luo, H. Guo, R.-D. Jiang, M.-Q. Liu, Y. Chen, X.-R. Shen, X. Wang, X.-S. Zheng, K. Zhao, Q.-J. Chen, F. Deng, L.-L. Liu, B. Yan, F.-X. Zhan, Y.-Y. Wang, G.-F. Xiao, Z.-L. Shi, A pneumonia outbreak associated with a new coronavirus of probable bat origin. *Nature* **579**, 270–273 (2020). doi:10.1038/s41586-020-2012-7 Medline
3. M. L. Holshue, C. DeBolt, S. Lindquist, K. H. Lofy, J. Wiesman, H. Bruce, C. Spitters, K. Ericson, S. Wilkerson, A. Tural, G. Diaz, A. Cohn, L. Fox, A. Patel, S. I. Gerber, L. Kim, S. Tong, X. Lu, S. Lindstrom, M. A. Pallansch, W. C. Weldon, H. M. Biggs, T. M. Uyeki, S. K. Pillai, Washington State 2019-nCoV Case Investigation Team, First Case of 2019 Novel Coronavirus in the United States. *N. Engl. J. Med.* **382**, 929–936 (2020). doi:10.1056/NEJMoa2001191 Medline
4. Q. Li, X. Guan, P. Wu, X. Wang, L. Zhou, Y. Tong, R. Ren, K. S. M. Leung, E. H. Y. Lau, J. Y. Wong, X. Xing, N. Xiang, Y. Wu, C. Li, Q. Chen, D. Li, T. Liu, J. Zhao, M. Liu, W. Tu, C. Chen, L. Jin, R. Yang, Q. Wang, S. Zhou, R. Wang, H. Liu, Y. Luo, Y. Liu, G. Shao, H. Li, Z. Tao, Y. Yang, Z. Deng, B. Liu, Z. Ma, Y. Zhang, G. Shi, T. T. Y. Lam, J. T. Wu, G. F. Gao, B. J. Cowling, B. Yang, G. M. Leung, Z. Feng, Early Transmission Dynamics in Wuhan, China, of Novel Coronavirus-Infected Pneumonia. *N. Engl. J. Med.* **382**, 1199–1207 (2020). doi:10.1056/NEJMoa2001316 Medline
5. N. Zhu, D. Zhang, W. Wang, X. Li, B. Yang, J. Song, X. Zhao, B. Huang, W. Shi, R. Lu, P. Niu, F. Zhan, X. Ma, D. Wang, W. Xu, G. Wu, G. F. Gao, W. Tan, China Novel Coronavirus Investigating and Research Team, A Novel Coronavirus from Patients with Pneumonia in China, 2019. *N. Engl. J. Med.* **382**, 727–733 (2020). doi:10.1056/NEJMoa2001017 Medline
6. N. Chen, M. Zhou, X. Dong, J. Qu, F. Gong, Y. Han, Y. Qiu, J. Wang, Y. Liu, Y. Wei, J. Xia, T. Yu, X. Zhang, L. Zhang, Epidemiological and clinical characteristics of 99 cases of 2019 novel coronavirus pneumonia in Wuhan, China: A descriptive study. *Lancet* **395**, 507–513 (2020). doi:10.1016/S0140-6736(20)30211-7 Medline
7. C. Huang, Y. Wang, X. Li, L. Ren, J. Zhao, Y. Hu, L. Zhang, G. Fan, J. Xu, X. Gu, Z. Cheng, T. Yu, J. Xia, Y. Wei, W. Wu, X. Xie, W. Yin, H. Li, M. Liu, Y. Xiao, H. Gao, L. Guo, J. Xie, G. Wang, R. Jiang, Z. Gao, Q. Jin, J. Wang, B. Cao, Clinical features of patients infected with 2019 novel coronavirus in Wuhan, China. *Lancet* **395**, 497–506 (2020). doi:10.1016/S0140-6736(20)30183-5 Medline
8. J. F. Chan, S. Yuan, K.-H. Kok, K. K.-W. To, H. Chu, J. Yang, F. Xing, J. Liu, C. C.-Y. Yip, R. W.-S. Poon, H.-W. Tsoi, S. K.-F. Lo, K.-H. Chan, V. K.-M. Poon, W.-M. Chan, J. D. Ip, J.-P. Cai, V. C.-C. Cheng, H. Chen, C. K.-M. Hui, K.-Y. Yuen, A familial cluster of pneumonia associated with the 2019 novel coronavirus indicating person-to-person transmission: A study of a family cluster. *Lancet* **395**, 514–523 (2020). doi:10.1016/S0140-6736(20)30154-9 Medline
9. R. Wölfel, V. M. Corman, W. Guggemos, M. Seilmaier, S. Zange, M. A. Müller, D. Niemeyer, T. C. Jones, P. Vollmar, C. Rothe, M. Hoelscher, T. Bleicker, S. Brünink, J. Schneider, R. Ehmann, K. Zwirglmaier, C. Drosten, C. Wendtner, Virological assessment of hospitalized patients with COVID-2019. *Nature* (2020). doi:10.1038/s41586-020-2196-x Medline
10. Z. Y. Yang, W. P. Kong, Y. Huang, A. Roberts, B. R. Murphy, K. Subbarao, G. J. Nabel, A DNA vaccine induces SARS coronavirus neutralization and protective immunity in mice. *Nature* **428**, 561–564 (2004). doi:10.1038/nature02463 Medline
11. T. Scobey, B. L. Yount, A. C. Sims, E. F. Donaldson, S. S. Agnihothram, V. D. Menachery, R. L. Graham, J. Swanstrom, P. F. Bove, J. D. Kim, S. Grego, S. H. Randell, R. S. Baric, Reverse genetics with a full-length infectious cDNA of the Middle East respiratory syndrome coronavirus. *Proc. Natl. Acad. Sci. U.S.A.* **110**, 16157–16162 (2013). doi:10.1073/pnas.1311542110 Medline
12. B. Yount, K. M. Curtis, E. A. Fritz, L. E. Hensley, P. B. Jahrling, E. Prentice, M. R. Denison, T. W. Geisbert, R. S. Baric, Reverse genetics with a full-length infectious cDNA of severe acute respiratory syndrome coronavirus. *Proc. Natl. Acad. Sci. U.S.A.* **100**, 12995–13000 (2003). doi:10.1073/pnas.1735582100 Medline

13. A. W. Chung, M. P. Kumar, K. B. Arnold, W. H. Yu, M. K. Schoen, L. J. Dunphy, T. J. Suscovich, N. Frahm, C. Linde, A. E. Mahan, M. Hoffner, H. Streeck, M. E. Ackerman, M. J. McElrath, H. Schuitemaker, M. G. Pau, L. R. Baden, J. H. Kim, N. L. Michael, D. H. Barouch, D. A. Lauffenburger, G. Alter, Dissecting Polyclonal Vaccine-Induced Humoral Immunity against HIV Using Systems Serology. *Cell* **163**, 988–998 (2015). doi:10.1016/j.cell.2015.10.027 Medline

14. C. Deleage, A. Schuetz, W. G. Alvord, L. Johnston, X.-P. Hao, D. R. Morcock, R. Rerknimitr, J. L. K. Fletcher, S. Puttamaswin, N. Phanuphak, R. Dewar, J. M. McCune, I. Sereti, M. Robb, J. H. Kim, T. W. Schacker, P. Hunt, J. D. Lifson, J. Ananworanich, J. D. Estes, Impact of early cART in the gut during acute HIV infection. *JCI Insight* **1**, e87065 (2016). doi:10.1172/jci.insight.87065 Medline

15. C. Deleage, S. W. Wietgrefe, G. Del Prete, D. R. Morcock, X.-P. Hao, M. Piatak Jr., J. Bess, J. L. Anderson, K. E. Perkey, C. Reilly, J. M. McCune, A. T. Haase, J. D. Lifson, T. W. Schacker, J. D. Estes, Defining HIV and SIV Reservoirs in Lymphoid Tissues. *Pathog. Immun.* **1**, 68–106 (2016). doi:10.20411/pai.v1i1.100 Medline

16. J. R. Lin, B. Izar, S. Wang, C. Yapp, S. Mei, P. M. Shah, S. Santagata, P. K. Sorger, Highly multiplexed immunofluorescence imaging of human tissues and tumors using t-CyCIF and conventional optical microscopes. *eLife* **7**, e31657 (2018). doi:10.7554/eLife.31657 Medline

17. M. Altfeld, T. M. Allen, X. G. Yu, M. N. Johnston, D. Agrawal, B. T. Korber, D. C. Montefiori, D. H. O'Connor, B. T. Davis, P. K. Lee, E. L. Maier, J. Harlow, P. J. R. Goulder, C. Brander, E. S. Rosenberg, B. D. Walker, HIV-1 superinfection despite broad $CD8^+$ T-cell responses containing replication of the primary virus. *Nature* **420**, 434–439 (2002). doi:10.1038/nature01200 Medline

18. K. A. Callow, H. F. Parry, M. Sergeant, D. A. Tyrrell, The time course of the immune response to experimental coronavirus infection of man. *Epidemiol. Infect.* **105**, 435–446 (1990). doi:10.1017/S0950268800048019 Medline

19. B. Rockx, T. Kuiken, S. Herfst, T. Bestebroer, M. M. Lamers, B. B. Oude Munnink, D. de Meulder, G. van Amerongen, J. van den Brand, N. M. A. Okba, D. Schipper, P. van Run, L. Leijten, R. Sikkema, E. Verschoor, B. Verstrepen, W. Bogers, J. Langermans, C. Drosten, M. Fentener van Vlissingen, R. Fouchier, R. de Swart, M. Koopmans, B. L. Haagmans, Comparative pathogenesis of COVID-19, MERS, and SARS in a nonhuman primate model. *Science* eabb7314 (2020). doi:10.1126/science.abb7314 Medline

ACKNOWLEDGMENTS

We thank B. Walker, A. Chakraborty, K. Reeves, B. Chen, J. Feldman, B. Hauser, T. Caradonna, S. Bondoc, C. Starke, C. Jacobson, D. O'Connor, S. O'Connor, N. Thornburg, E. Borducchi, M. Silva, A. Richardson, C. Caron, and J. Cwiak for generous advice, assistance, and reagents. **Funding:** We acknowledge support from the Ragon Institute of MGH, MIT, and Harvard, Mark and Lisa Schwartz Foundation, Beth Israel Deaconess Medical Center, Massachusetts Consortium on Pathogen Readiness (MassCPR), Bill & Melinda Gates Foundation (INV-006131), Janssen Vaccines & Prevention BV, and the National Institutes of Health (OD024917, AI129797, AI124377, AI128751, AI126603 to D.H.B.; AI135098 to A.J.M.; AI007387 to L.H.T.; AI007151 to D.R.M.; AI146779 to A.G.S.; 272201700036I-0-759301900131-1, AI100625, AI110700, AI132178, AI149644, AI108197 to R.S.B.; CA225088 to P.K.S.; and OD011092, OD025002 to J.D.E.). We also acknowledge a Fast Grant, Emergent Ventures, Mercatus Center at George Mason University to A.J.M. and a Burroughs Wellcome Fund Postdoctoral Enrichment Program Award to D.R.M. **Author contributions:** D.H.B., H.A., and M.G.L. designed the study. A.C., J.L., K.M., N.B.M., L.P., L.H.T., J.Y., P.A., E.A.B., G.D., M.S.G., X.H., C.J.D., N.K., Z.L., M.A.L., L.F.M., and J.P.N. performed the immunologic and virologic assays. A.J.M., Z.M., M.N., K.B.S., M.T. L.M.W., S.D., A.D.M., P.K.S., and J.D.E. performed the pathology studies. D.R.M. and R.S.B. performed the live virus neutralization assays. C.A., S.F., J.S.B., M.D.S., and G.A. performed the antibody phenotyping. L.P., A.V.R., J.G., T.T., K.B., A.C., B.F., R.B., E.T., J.V., H.A., and M.G.L. led the clinical care of the animals and performed the virologic assays. R.Z. and F.W. participated in study design and interpretation of data. A.G.S. and B.C. provided purified proteins. D.H.B. wrote the paper with all co-authors. **Competing interests:** The authors declare no competing financial interests. G.A. is an inventor on patent application WO 2017/184733 A1 submitted by Massachusetts General Hospital that covers systems serology. R.Z. and F.W. are employees of Janssen Vaccines & Prevention BV. **Data and materials availability:** All data are available in the manuscript or the supplementary material. Virus stocks are available from D.H.B. under a material transfer agreement with Beth Israel Deaconess Medical Center.

SUPPLEMENTARY MATERIALS

science.sciencemag.org/cgi/content/full/science.abc4776/DC1
Materials and Methods
Table S1
Figs. S1 to S11

26 April 2020; accepted 16 May 2020
Published online 20 May 2020
10.1126/science.abc4776

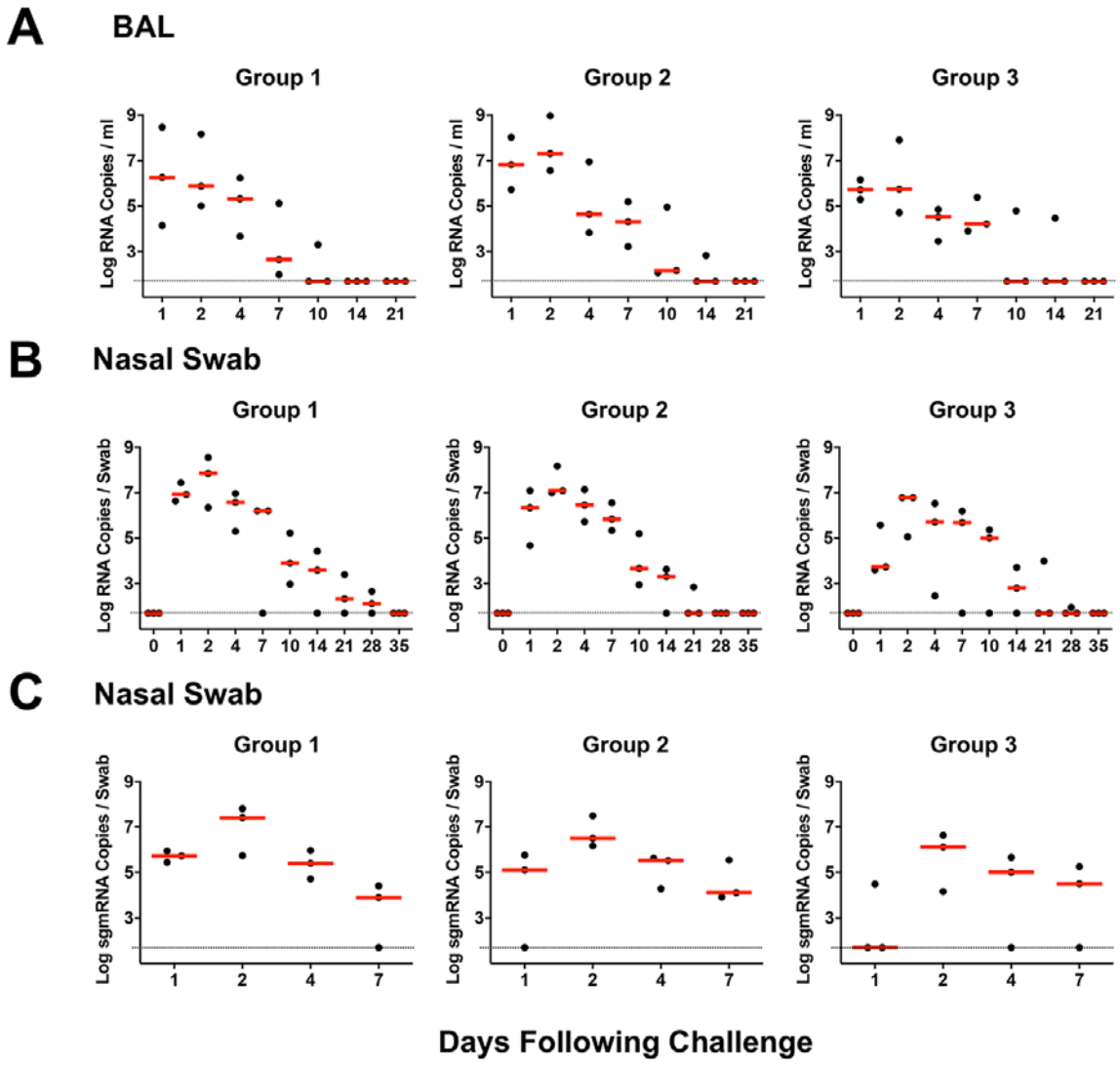

Fig. 1. Viral loads in SARS-CoV-2 challenged rhesus macaques. Rhesus macaques were inoculated by the intranasal and intratracheal route with 1.1×10^6 PFU (Group 1; N = 3), 1.1×10^5 PFU (Group 2; N = 3), or 1.1×10^4 PFU (Group 3; N = 3) SARS-CoV-2. (**A**) Log_{10} viral RNA copies/ml (limit 50 copies/ml) were assessed in bronchoalveolar lavage (BAL) at multiple timepoints following challenge. (**B** and **C**) Log_{10} viral RNA copies/swab (B) and log_{10} sgmRNA copies/swab (limit 50 copies/swab) (C) were assessed in nasal swabs (NS) at multiple timepoints following challenge. Red horizontal bars reflect median viral loads.

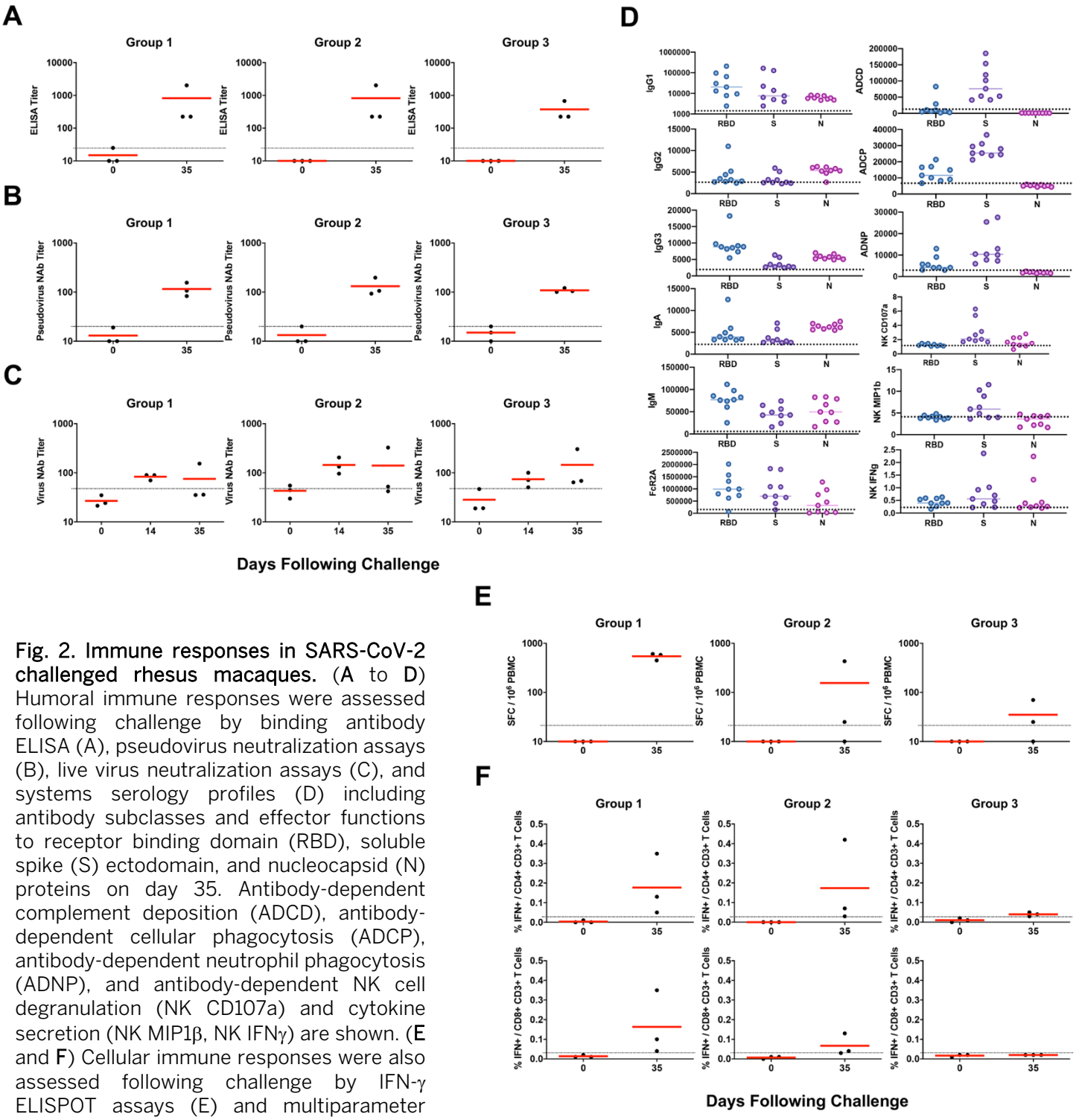

Fig. 2. Immune responses in SARS-CoV-2 challenged rhesus macaques. (**A** to **D**) Humoral immune responses were assessed following challenge by binding antibody ELISA (A), pseudovirus neutralization assays (B), live virus neutralization assays (C), and systems serology profiles (D) including antibody subclasses and effector functions to receptor binding domain (RBD), soluble spike (S) ectodomain, and nucleocapsid (N) proteins on day 35. Antibody-dependent complement deposition (ADCD), antibody-dependent cellular phagocytosis (ADCP), antibody-dependent neutrophil phagocytosis (ADNP), and antibody-dependent NK cell degranulation (NK CD107a) and cytokine secretion (NK MIP1β, NK IFNγ) are shown. (**E** and **F**) Cellular immune responses were also assessed following challenge by IFN-γ ELISPOT assays (E) and multiparameter intracellular cytokine staining assays (F) in response to pooled S peptides. Red and horizontal bars reflect mean responses.

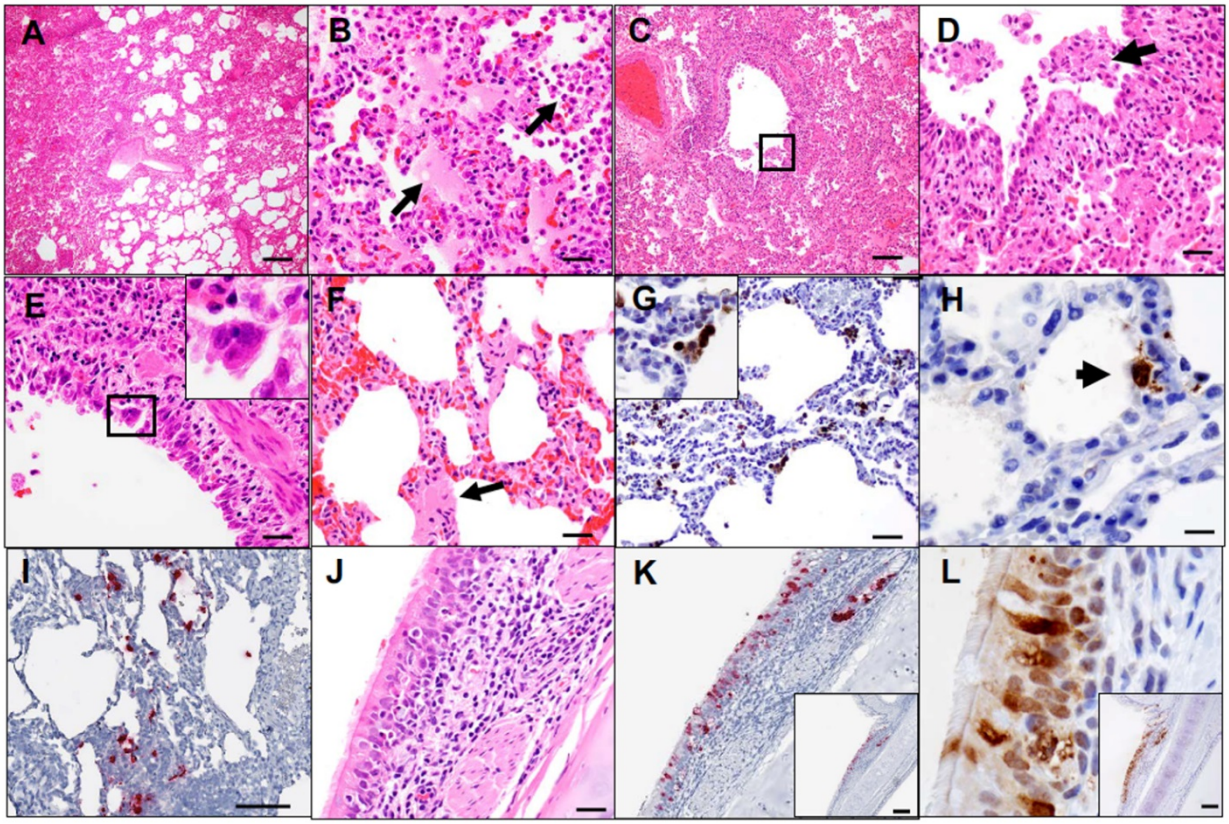

Fig. 3. SARS-CoV-2 induces acute viral interstitial pneumonia. (**A** to **F**) H&E sections of fixed lung tissue from SARS-CoV-2 infected rhesus macaques 2 days following challenge showing interstitial edema and regional lung consolidation (A), intra-alveolar edema and infiltrates of neutrophils (B), bronchiolar epithelial sloughing and necrosis [(C) and (D)], bronchiolar epithelial syncytial cell formation (E), and hyaline membranes within alveolar septa (F). (**G** and **H**) IHC for SARS nucleocapsid showing virus infected cells within interstitial spaces including a viral syncytial cell within the lumen (G) and virus infected alveolar lining cells (H). (**I**) Inflammatory infiltrate showing multiple cells containing SARS-CoV-2 RNA by RNAscope in situ hybridization. (**J** to **L**) bronchial respiratory epithelium showing inflammation within the submucosa and transmigration of inflammatory cells into the ciliated columnar respiratory epithelium of a bronchus (J), SARS-CoV-2 RNA (K), and SARS nucleocapsid (L). Scale bars (A) = 200 microns; (C, I, K-L) = 100 micron; (G) = 50 micron; (B, D-F, J) = 20 microns, and (H) = 10 microns. H&E = hematoxylin and eosin; IHC = immunohistochemistry; RNAscope = SARS-CoV-2 RNA staining.

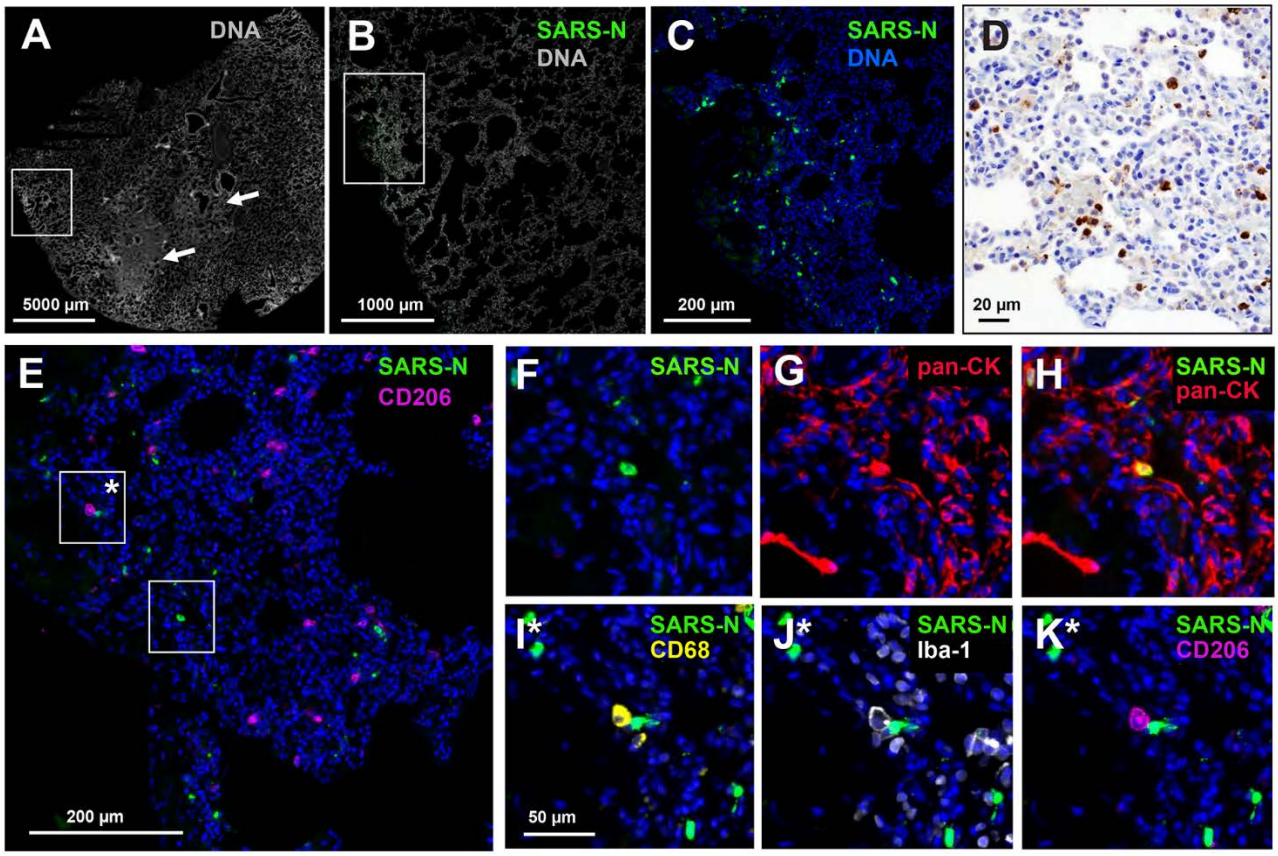

Fig. 4. SARS-CoV-2 infects alveolar epithelial cells in rhesus macaques. Cyclic immunofluorescence (CyCIF) staining of fixed lung tissue from SARS-CoV-2 infected rhesus macaques 2 days following challenge. (**A**) Whole slide image of a lung stained with Hoechst 33342 to visualize cell nuclei (greyscale); regions of nuclear consolidation (arrows), and foci of viral replication (box) are highlighted. (**B**) Higher magnification image of inset box in (A) showing staining for SARS nucleocapsid protein (SARS-N; green) and cell nuclei (grey scale). (**C**) Higher magnification image of inset box in (B) showing SARS-N (green) and cell nuclei (blue). (**D**) Bright-field IHC for SARS-N from corresponding lung region depicted in (C). (**E** to **K**) CyCIF staining for DNA (blue; all panels) and SARS-N [(E), (F), and (H-K); green], CD206 [(E) and (K); magenta], pan-cytokeratin (pan-CK) [(G) and (H); red], CD68 (I; yellow), or Iba-1 (J; greyscale) showing virus infected epithelial cells and macrophages near an infected epithelial cell. Scale bars (F-K) = 50 microns.

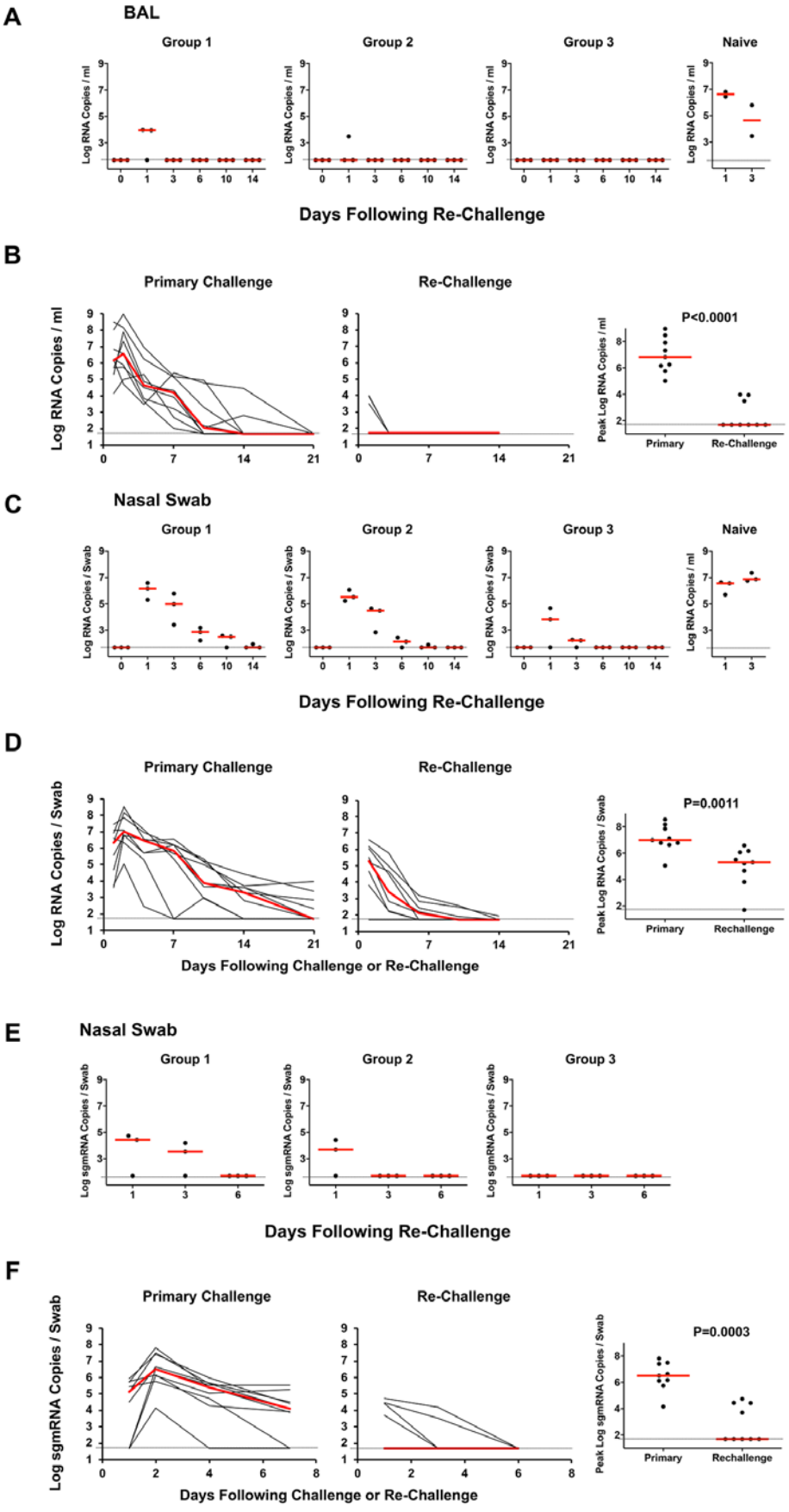

Fig. 5. Viral loads following SARS-CoV-2 rechallenge in rhesus macaques. On day 35 following initial infection (Fig. 1), rhesus macaques were rechallenged with SARS-CoV-2 by the intranasal and intratracheal route with 1.1×10^6 PFU (Group 1; N = 3), 1.1×10^5 PFU (Group 2; N = 3), or 1.1×10^4 PFU (Group 3; N = 3). Three naïve animals were included as a positive control in the rechallenge experiment. (**A**) Log_{10} viral RNA copies/ml (limit 50 copies/ml) were assessed in bronchoalveolar lavage (BAL) at multiple timepoints following rechallenge. One of the naïve animals could not be lavaged. (**B**) Comparison of viral RNA in BAL following primary challenge and rechallenge. (**C** and **E**) Log_{10} viral RNA copies/ml (C) and log_{10} sgmRNA copies/swab (limit 50 copies/ml) (E) were assessed in nasal swabs (NS) at multiple timepoints following rechallenge. (**D** and **F**) Comparison of viral RNA (D) and sgmRNA (F) in NS following primary challenge and rechallenge. Red horizontal bars reflect median viral loads. P-values reflect two-sided Mann-Whitney tests.

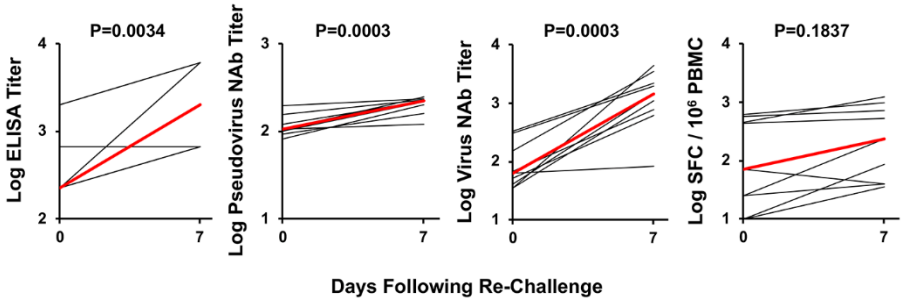

Fig. 6. Anamnestic immune responses following SARS-CoV-2 rechallenge in rhesus macaques. Binding antibody ELISAs, pseudovirus neutralization assays, live virus neutralization assays, and IFN-γ ELISPOT assays are depicted prior to and 7 days following SARS-CoV-2 rechallenge. Red lines reflect mean responses. P-values reflect two-sided Mann-Whitney tests.